PtSe$_2$ and black phosphorus employed for sensitivity improvement in the surface plasmon resonance sensor

Bhishma Karki[1,2] · Gufranullah Ansari[3] · Arun Uniyal[4] · Vivek Srivastava[5]

Abstract

The analysis aims to enhance the sensitivity of the surface plasmon resonance-based
sensor. The proposed sensor consists of a single layer of Ag metal, black phosphorus (BP), and Platinum diselenide (PtSe$_2$). The thickness of the Ag metal is considered as 45 nm. The study was carried out using attenuated total reflection. The refractive index of the sensor changes when analyte or biomolecules comes in contact with the sensing layer. The thickness of the BP layer has been taken as 0.34 nm. The maximum sensitivity of the sensor is achieved for one layer of PtSe$_2$ and two layers of BP. The calculated performance parameters, sensitivity, figure of merit, and detection accuracy, are 275.2 Degree/RIU, 43.1 RIU^{-1}, and 0.16 Degree^{-1}, respectively. The sensitivity of the proposed sensor is 1.38 times the conventional sensor.

Keywords Surface plasmon resonance · PtSe$_2$ · Black phosphorus · Sensitivity enhancement

1 Introduction

Surface plasmons (SPs) are dense oscillating electrons cloud propagation at the metal and dielectric interface. They are useful for the detection of molecular properties of the sensing medium, such as size, concentration, and the analyte in biology and biochemistry [1][1][1]. When an analyte interacts with the biorecognition elements (BRE) of the surface plasmon resonance (SPR) sensor, the BRE element's biomolecular bonding enhances, and the refractive index of the sensing medium changes significantly [4]. This phenomenon causes a change in the surface plasmons'

propagation constant, allowing a significant shift in the resonance curve [5][5]. The necessary condition for any good sensor must show high sensitivity, low full width at half maximum (FWHM), high detection accuracy, repeatability and reproducibility, and high stability over time in different chemical and physical conditions [7][7].

To design an SPR-based sensor, Kretschmann is the most widely used configuration [9][9][9][9]. The sensor's sensitivity is analyzed at the dip in the resonance curve, where the resonance angle is measured. In the dip, the absorbance of the light is maximum, and reflectivity is minimum. Here angle interrogation technique is used for the analysis of the sensor. The input signal of wavelength $\lambda = 633$nm is used here. The conventional Kretschmann configuration is modified by stacking the layer of two-dimensional (2-D) material or artificially developed heterostructure material such as graphene, black phosphorus, barium titanate, and tin selenide. These modified sensor heterostructures show enhanced sensitivity and better performance than the conventional sensor [13][13][13][13].

In traditional sensors, silver (Ag) metal layers are widely utilized [17][17]. Near the infrared region, the resonance curve of Ag metal shows a significant dip, indicating that the sensor produces high sensitivity [19]. The other advantages of Ag metal-based sensors include that they are more accurate than gold, have a narrower

✉ Bhishma Karki
magnum.photon@gmail.com

1 Department of Physics, Tri-Chandra Multiple Campus, Tribhuvan University, Kathmandu 44600, Nepal

2 National Research Council Nepal, New Baneshwor-10, Kathmandu 44600, Nepal

3 Dr. Shanti Swarup Bhatnagar University Institute of Chemical Engineering & Technology, Panjab University, Sector 14, Chandigarh, U.T. 160014, India

4 Department of ECE, IT Gopeshwar, Chamoli 246424, Uttarakhand, India

5 Department of Mechanical Engineering, ABES Engineering College, Ghaziabad UP, 201009, India

resonance curve with higher contrast, and have a lower FWHM than gold [20][20]. Its demerit includes low stability since it is readily oxidized when exposed to air or water [22]. The sensor's sensitivity reduces due to the oxidation of the Ag layer. A BRE reduces the oxidation problem and improves the sensor's performance [23].

After experimental analysis, it is found that 2-D materials such as black phosphorus (BP) and graphene as BREs can improve the sensitivity and performance characteristics of the SPR sensors [24][24][24][24][24]. Some important points about BP are that its response time is very low compared to the other 2-D materials, which allows sensing the parts per billion quantities of the analyte, and adsorption energy is also very high compared to graphene, WS_2, and MoS_2. Furthermore, BP has a puckered lattice arrangement, giving it a substantially higher surface-to-volume ratio than other 2-D materials [29]. As a result, BP may be ideal for biomolecule binding. The electrical and optical properties of the BP have been analyzed experimentally. Cai et al. observed that the effective carrier mass, energy band gap, and work function depending on the thickness of the BP material, which decreases with the increase in thickness. But the only drawback is the stability issue, which is unstable in air and water [30]. Therefore, BP is the best suitable material for gas sensing. Rahman et al. theoretically investigated a sensor using BK7 prism, $PtSe_2$, and 2-D materials, and a maximum sensitivity of 194 Degree/RIU are achieved [31]. Fouad et al. proposed a sensor based on the SPR technique using silver (Ag) and barium titanate ($BaTiO_3$) and achieved maximum sensitivity of 280 Degree/RIU [32]. An SPR-based gas sensor was proposed by Shrivastava and Jha using a bilayer of BP and MoS_2 layers. They attained a maximum sensitivity for this was around 110 Degree/RIU [33]. Kumela et al. proposed a plasmonic sensor with increased sensitivity that models the optical characteristics of metal nanoparticles using both classical and quantum approaches [34].

$PtSe_2$ has extraordinary optical and electromechanical properties. Due to its strong interlayer contact and quantum confinement effect, it has a large tunable energy band gap [35]. Furthermore, it exhibits an outstanding transition characteristic from semimetal to semiconductor while transitioning from bulk to a few layers. It also provides toxicity resistance and chemical inertness, making it a potential material for sensing applications [13].

In this work, a hybrid multilayer sensor based on Ag metal, $PtSe_2$, and black phosphorus has been designed to analyze the conventional structure comprehensively. Here angular interrogation method based on attenuated total reflection (ATR) is used to analyze the sensor. The sensor's performance is based on parameters like sensitivity,

detection accuracy, the figure of merit, etc. The manuscript is structured in the following manner: Section 2 consists of design consideration and theoretical cum mathematical modeling of the proposed sensor. Section 3 explains the results and discussion, while the conclusion of the work is provided in section 4.

2 Theoretical analysis and mathematical modeling of the sensor

2.1 Design analysis and theoretical modeling

Figure 1 consists of the schematic of the proposed sensor, a modified Kretschmann configuration. The thickness of the Ag layer 45 nm is taken and deposited over the prism. The dispersion profile of the metal is computed using the Drude–Lorentz model and given as [9]:

$$n_{Ag} = \left(1 - \frac{\lambda^2 * \lambda_c}{\lambda_p^2 (\lambda_c + \lambda * i)} \right)^{1/2} \tag{1}$$

where λ_c and λ_p are the collision and plasma wavelength of the material, and its values are 1.4541×10^{-7} and 17.614×10^{-6}, respectively [36]. The proposed configuration utilizes the BK7 coupling prism. The refractive index of the BK7 is low, so it provides better sensitivity. Here monochromatic plane polarizes TM optical signal to operate the proposed sensor. The refractive index of the prism is calculated using this formula [11]:

$$n_{BK7} = \left(\frac{1.03961212^2}{2 - 0.00600069867} + \frac{0.231792344^2}{2 - 0.0200179144} + \frac{1.0104694^2}{2 - 103.560653} + 1 \right)^{\frac{1}{2}} \tag{2}$$

The metal layer of the sensor is attached to the thin layer of $PtSe_2$; after that, a thin layer of black phosphorus is spread over it. The heterostructure of transition metal diselenide /2-D materials is taken as an affinity layer to interact with the sensing layer or analyte, simultaneously preventing the oxidation of the metal. Design parameters and their respective refractive index (RI) are given in Table 1. The refractive index of the sensing medium is taken as 1.33, and δn is the variation in the RI of the sensing medium when the analyte comes in contact with it.

2.2 Mathematical modeling

To analyze the sensitivity/performance of the sensor, first, investigate the reflection intensity of the TM-polarized light at the sensor's detector. The mathematical modeling of the multilayer configuration of the sensor can be fulfilled by analyzing the Drude–Lorentz model/Fresnel equation and transfer matrix method (TMM). This study uses no

Fig. 1 Multilayered sensor design for sensing applications
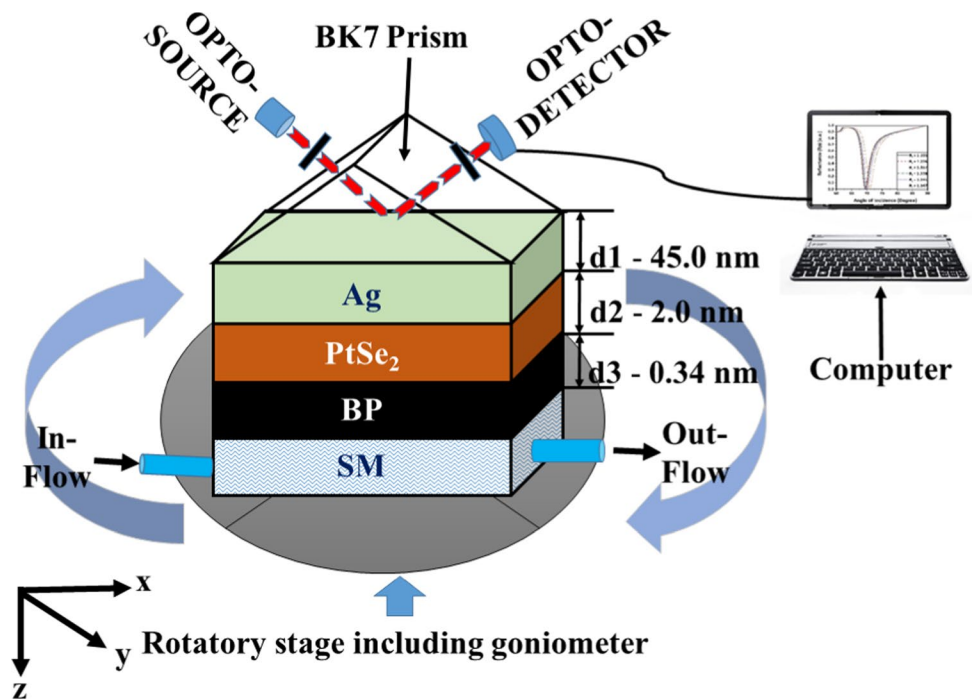
Table 1 Dimension and refractive index of the material used in the sensor

Material	Thickness of the layer	RI at $\lambda = 633nm$	References
Prism BK7	–	1.5151	[37]
Ag layer (D_1)	45 nm	$0.056206 + i * 4.2776$	[38]
PtSe$_2$ (D_2)	2 nm	$2.9189 + i * 0.9593$	[31]
	3.3 nm	$2.8528 + i * 1.1129$	
	4.4 nm	$3.0233 + i * 1.4967$	
Black phosphorus (D_3)	0.65 nm	$3.531 - i * 0.04087$	[24]
Sensing medium	–	$1.33 + \delta n$	[39]

approximation method of TMM, which provides the best results [40]. MATLAB is used to estimate the SPR modulation analogy. To proceed with the mathematical modeling, some parameters need to specify. The individual thickness of each layer is described as 'd_k,' are stacked in the Z-direction. The sufficient condition for surface plasmon resonance is when the propagation constant of the evanescent wave matches with the surface plasmon by taking the specific value of the angle. This condition is known as wavevector matching because the incident light wavevector matches with the surface plasmon wavevector [41].

$$\frac{2\pi}{\lambda} n_{BK7} \sin\theta = Re(\beta_{SP}) \tag{3}$$

where θ is the angle of incidence, n_{BK7} is the RI of the prism, β_{SP} is the propagation constant of surface plasmon, and

numerically it can be written as $\left(\frac{2\pi}{\lambda} \sqrt{\frac{\varepsilon_m \varepsilon_s}{\varepsilon_m + \varepsilon_s}} \right)$. It is necessary to generate surface plasmon momentum, and energy must be conserved. The relation between angular frequency and wavevector in the X-direction can be written as:

$$k_x = \frac{\omega}{c} \sqrt{\frac{\varepsilon_1 \varepsilon_2}{\varepsilon_1 + \varepsilon_2}} \tag{4}$$

Here ε_1 and ε_2 denote the permittivity of the first two mediums of our proposed SPR sensor.

Drude–Lorentz's model shows the dependency of the wavelength of an incident optical signal on the dielectric constant of the metal. The refractive index of the BK7 prism is estimated using the Sellmeier equation. The transfer matrix method is used to compute the reflectivity of the TM-polarized light. The tangential component of the light at the metal surface is given as:

$$\begin{bmatrix} A_1 \\ B_1 \end{bmatrix} = M_2 M_3 M_4 \ldots\ldots\ldots M_{-1} \begin{bmatrix} A_{N-1} \\ B_{N-1} \end{bmatrix} = M \begin{bmatrix} A_{N-1} \\ B_{N-1} \end{bmatrix} \tag{5}$$

Here A_1 and B_1 are tangential components of the electric and magnetic fields at the first layer's surface. Similarly, electric and magnetic field components at the Nth layer's boundary are given as A_{N-1} and B_{N-1} respectively. M shows the characteristic transfer matrix of the N–layered configuration as follows [42]:

$$M = \prod_{K=2}^{N-1} M_K = \begin{bmatrix} M_{11} & M_{12} \\ M_{21} & M_{22} \end{bmatrix} \qquad (6)$$

where

$$M_K = \begin{bmatrix} \cos(\beta_k) & -i\sin(\beta_k)/q_k \\ -iq_k\sin(\beta_k) & \cos(\beta_k) \end{bmatrix} \qquad (7)$$

where q_k and β_k can be written as $q_k = \sqrt{\left(\frac{\mu_k}{\varepsilon_k}\right)}\cos\theta_k$ and $\beta_k = \frac{2\pi}{\lambda}n_k\cos\theta_k(d_k)$, respectively.

After simplifying the equations mentioned above, the reflection coefficient is written as [43]:

$$R = |r|^2 = \left(\frac{(M_{11} + M_{12}q_N)q_1 - (M_{21} + M_{22}q_N)}{(M_{11} + M_{12}q_N)q_1 + (M_{21} + M_{22}q_N)} \right) \qquad (8)$$

The sensitivity is the necessary parameter of the sensor and shows how resonance angle varies with respect to changes in the refractive index of the sensing medium; more precisely, it is said to be the limit of detection. The sensitivity should be high for the sensor, and it is defined as:

$$S = \frac{\delta\theta_{res}}{\delta n} \text{ (in Degree/RIU)} \qquad (9)$$

where $\delta\theta_{res}$ is the shift in the resonance angle of the incidence and δn is the variation in the refractive index of the sensing medium. The figure of merit (FoM) is another important parameter for the sensor, it shows the sensor's resolution, and its high value is desirable. FoM is defined as:

$$\text{FoM} = \frac{S}{\text{FWHM}} \text{(in 1/RIU)} \qquad (10)$$

For the best performance of the SPR sensor, FWHM should be low. So, the resonance curve should be narrow and sharp. Detection accuracy (DA) is computed as the reciprocal of the FWHM (1/FWHM). The FoM is a useful parameter to show the sensor's performance because it combines the result of sensitivity and FWHM.

3 Results and discussion

To demonstrate the enhancement in sensitivity performance, the plots between the reflectance of the structure and incidence angle at distinct refractive indexes (1.33 and 1.335) of
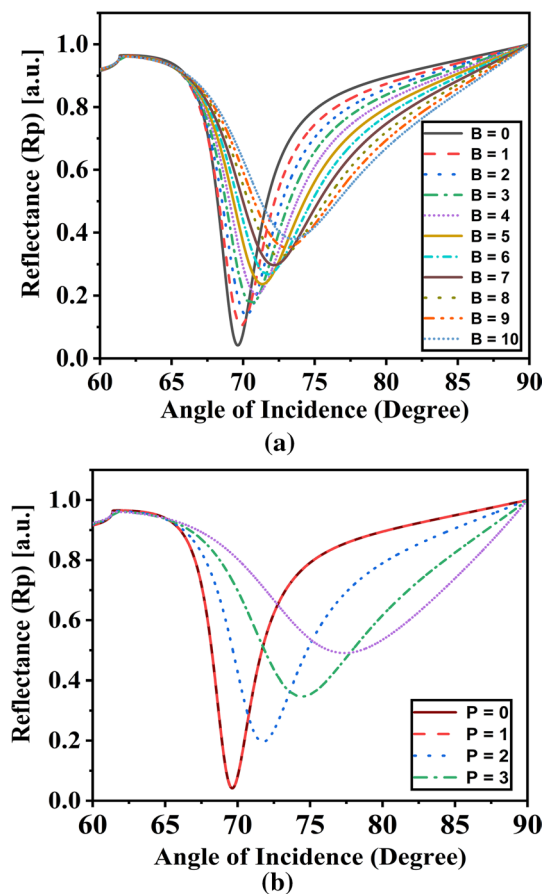

Fig. 2 Input (angle of incidence) relationship with output (reflectance) for **a** $P = 0, B = 0$ **b** $P = 0, B = 1$ **c** $P = 1, B = 0$ **d** $P = 1, B = 1$
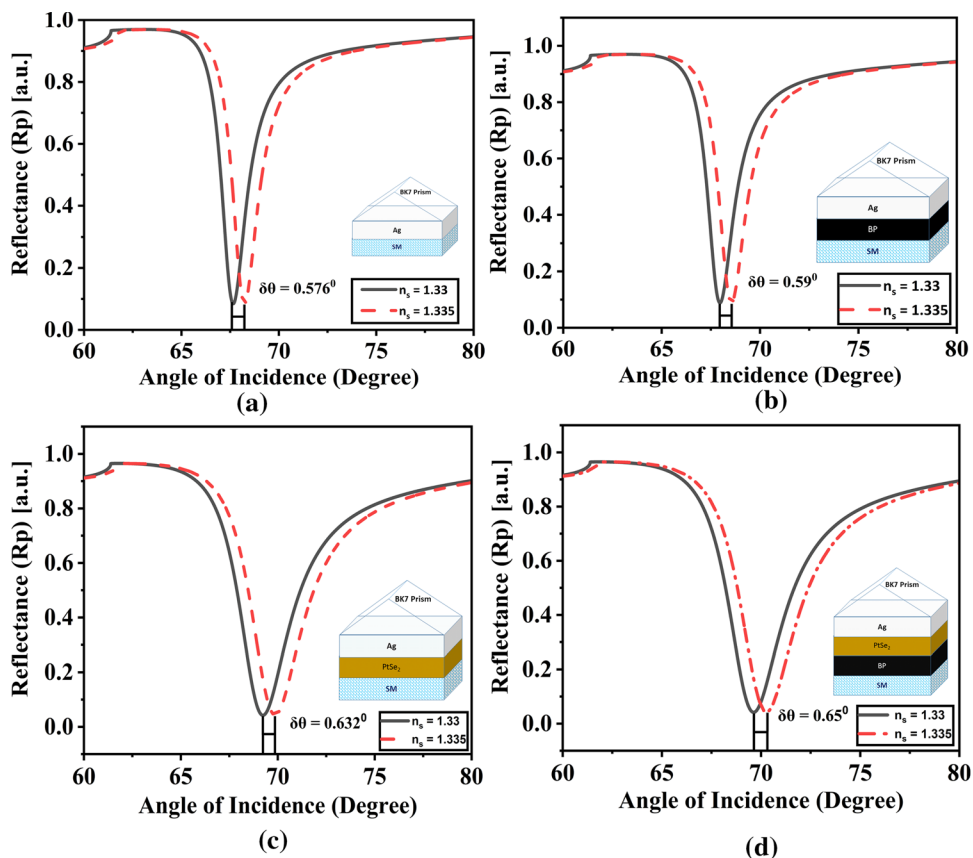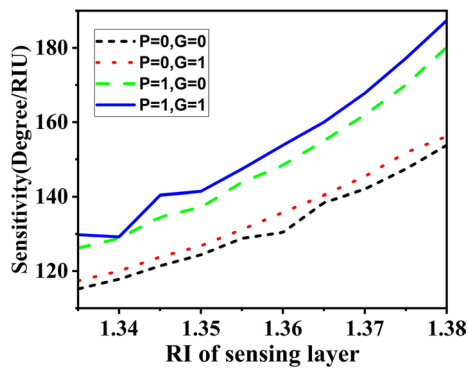
Fig. 3 Variation in sensitivity with the variation in RI of the sensing layer
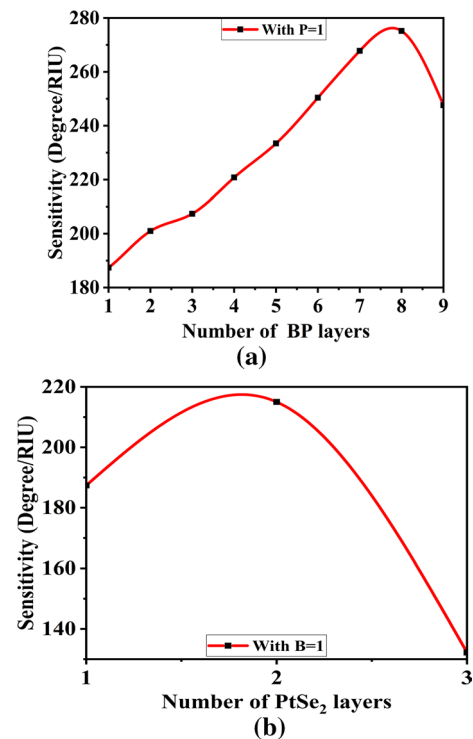
the sensing medium are shown in Fig. 2. For first Fig. 2a, it indicates the traditional SPR sensor setup, with the absence of both layers of PtSe$_2$ and BP ($P = 0, B = 0$). Our study demonstrated that the reflectance exhibits a sharp dip at a specific angle range due to the stimulation of SPR. This event shows that the stimulating SPR absorbs the incident light in our sensor setup. Further, with the molecule's cooperation,

the refractive index of the sensing medium changes. With this setup, the change in resonance angle ($\Delta\theta = 0.576°$) and sensitivity is calculated by ($S = 115.2$ Degree/RIU) as in equation 9. Figure 2b indicates a single BP layer ($B = 1$) and no PtSe$_2$ layer ($P = 0$); the other parameters were kept constant as in the previous condition. The values for $\Delta\theta = 0.59°$ and S = 118 Degree/RIU) are calculated. The sensitivity increases with the presence of a single BP layer when compared with Fig. 2a without BP. The next case, shown in Fig. 2c, gives the change in resonance angle and sensitivity ($\Delta\theta = 0.632°$ and $S = 126.4$ Degree/RIU) and with the presence of PtSe$_2$ layer and absence of BP layer.

Further, the presence of both layers of PtSe$_2$ and BP ($P, B = 1$) is shown in Fig. 2d. With the modification in the reflectance dip, the sensitivity increases to 0.65°, and the change in resonance angle comes out to be 130 Degree/RIU. We can see the alteration in the resonance angle of the sensor in our construction is higher than the typical SPR structure due to the addition of the PtSe$_2$ layer and the BP layer. Only a coupling prism and a metal (Ag) layer make up the typical SPR structure. As a result, we may conclude that combining PtSe$_2$ and a BP layer to our SPR sensor improves its sensitivity significantly when compared to a standard construction (Figure 2a). The above analysis shows that the sensing layer's RI can regulate the sensor's sensitivity.

Fig. 4 Plots showing the functionality of reflectance with the angle of incidence **a** for mono-PtSe$_2$ layer ($P = 1$) and varying BP layers (0 to 10) and **b** for mono-BP layer ($B = 1$) and varying PtSe$_2$ layers (0 to 3)

Fig. 5 Sensitivity variation with **a** number of BP layers (1 to 9) for $P = 1$ and **b** number of PtSe$_2$ layers (1 to 3) for $B = 1$
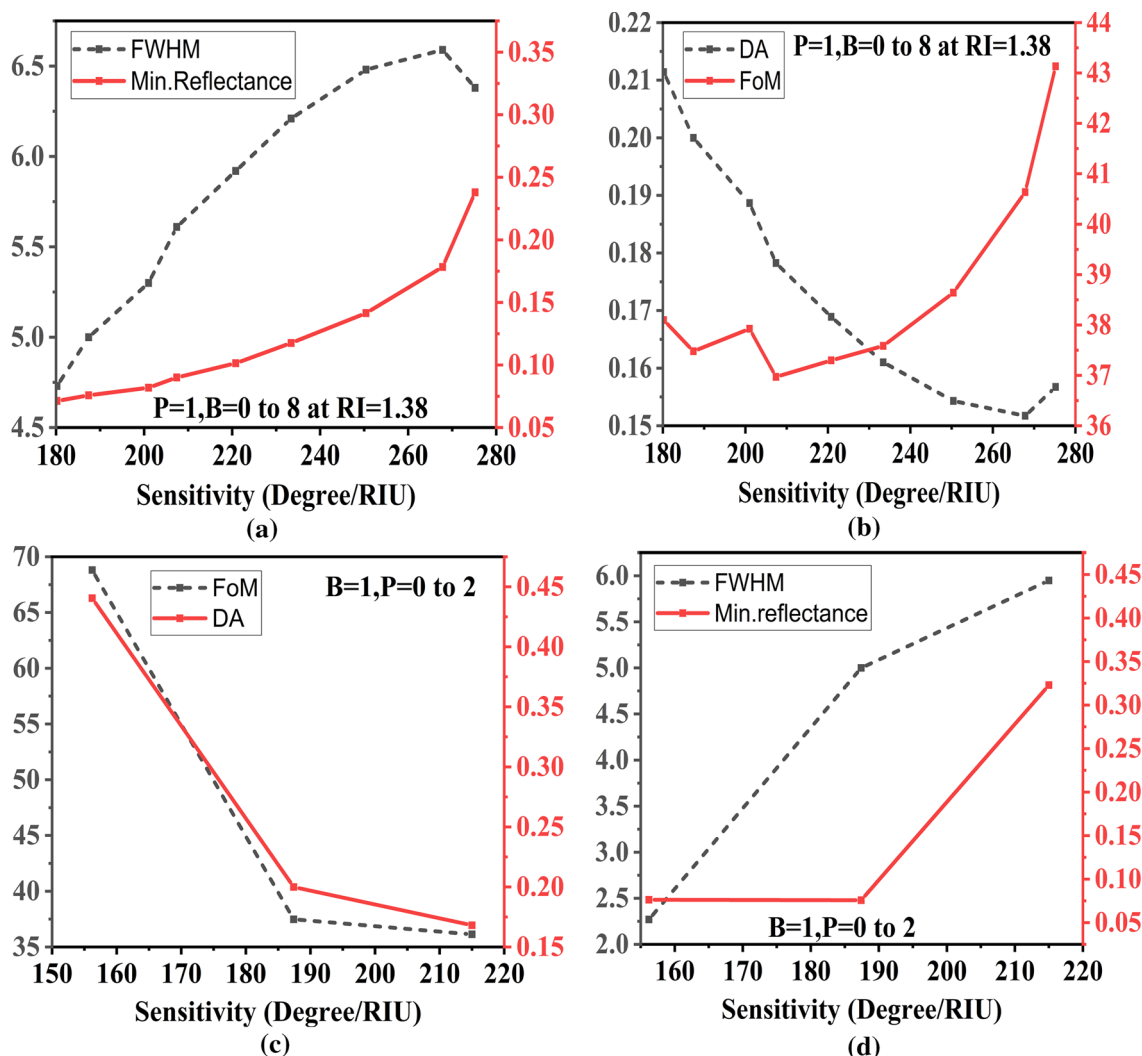
Fig. 6 **a**, **d** Different performance parameters analysis. For $P = 1, B = 0$ *to* 8 layers **a** Plot between FWHM and R $_{min}$ **b** Plot between DA and FoM. For $B = 1$ *and* $P = 0$ *to* 2 **c** Plot between FoM and DA and **d** Plot between FWHM and R $_{min}$

In Fig. 3, we also plot the dependence of the sensor's sensitivity on the sensing layer's refractive index to better understand the augmentation of the sensor's sensitivity by PtSe$_2$ and BP layers. The refractive index range of the sensing medium is taken from 1.33 to 1.38, with 0.005 variations in between. With the increase in refractive index, the sensitivity enhances significantly; for P = 0, G = 0, the sensitivity varies from 115.2 Degree/RIU) to 153.8 Degree/RIU) then for P = 0, B = 1 it varies to 156.2 Degree/RIU) from 117.4 Degree/RIU). In the next case, when P = 0, B = 1, the sensitivity reaches 180.2 Degree/RIU) maximum. Lastly, for P = B = 1 the highest sensitivity value is achieved as 187.4 Degree/RIU). This analysis signifies that after the introduction of PtSe$_2$ and the BP layer to the structure, the sensitivity increases from 153.8 Degree/RIU) to 187.4 Degree/RIU).

Further, we expand this study to a greater extent by seeing the impact of further addition of PtSe$_2$ and BP layer on the sensitivity of the proposed sensor. First, after adding the BP layer with a constant PtSe$_2$ layer (P = 1), its impact is observed on the sensitivity, as in Fig. 4a. Increasing the number of BP layers can improve reflectance. Furthermore, when the number of BP layers increases, a shift in reflectance dip is observed for a larger incidence angle, implying that the sensor's sensitivity increases. From Fig. 4b, the impact of adding a PtSe$_2$ layer on the sensor's sensitivity is observed while keeping one BP layer. It can be seen from the above plots (Fig. 4a and b) that the SPR curve dip gets wider with the increasing number of BP and PtSe$_2$ layers. It signifies that the measurement is complicated at a near resonance angle, which further impacts the sensors' accuracy. The prior discussion gives us the concept that by increasing the number of layers of BP and PtSe$_2$, the sensitivity increases to a

Fig. 7 **a**–**c** Electric field distribution as a function of distance from prism interface for PtSe$_2$ thickness, D$_2$ **a** 2 nm, **b** 3.3 nm, and **c** 4.4 nm
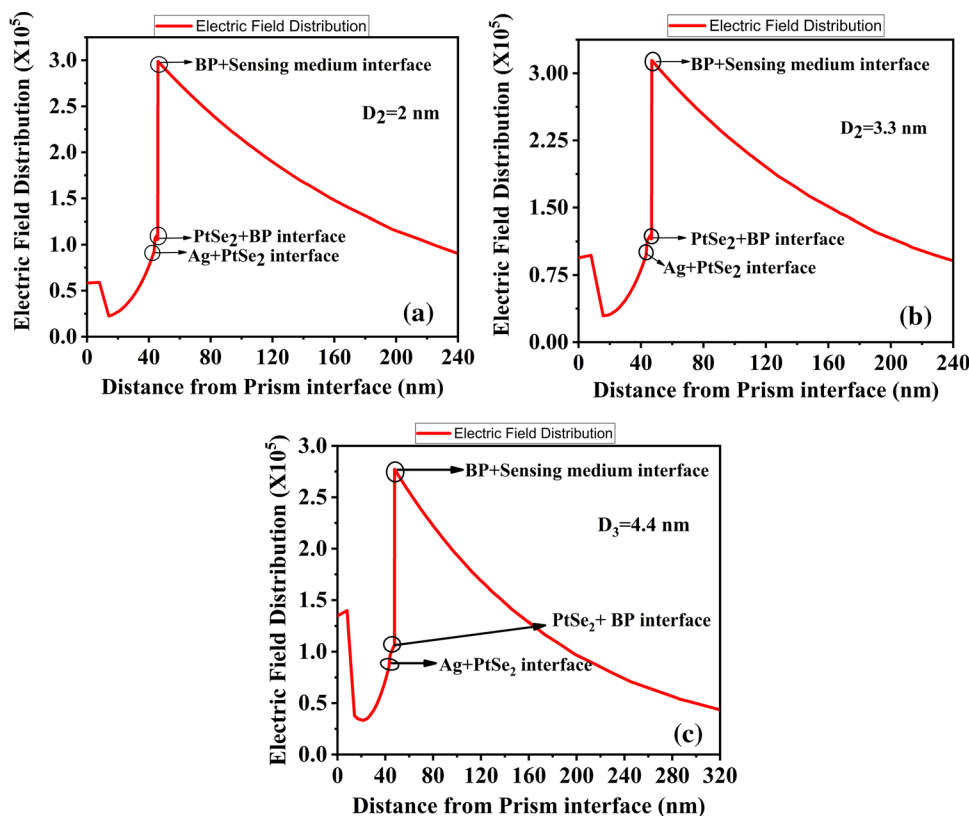
Table 2 Comparative survey of present work with earlier reported works

Wavelength	Design configuration	Sensitivity	DA	FoM	References
632.8 nm	BK7+ (ZnO, Ag, Au, Graphene)	76	–	–	[44]
632.8 nm	BK7+(Au, WSe$_2$)	179.32	0.17	–	[45]
633 nm	BK7+(Ag, BlueP, MoS$_2$)	230.66	1.04	34.58	[46]
633 nm	BK7+(Au, Al$_2$O$_3$, WS$_2$)	227.50	1.1123	28.26	[47]
633 nm	BK7+(Au, MoS$_2$, Au, graphene)	182	–	–	[48]
633 nm	BK7+(Ag/Au, PtSe$_2$)	165	0.1412	14.12	[13]
633 nm	BK7+ (Ag, PtSe$_2$, BP)	275.2	0.16	43.1	Present work

greater extent. The absorption of biomolecules is higher for BP as compared to PtSe$_2$. With the increase of BP layers, its effect on the reflectance is observed, which is greater than in the other layer's case. Fig. 5a gives the sensitivity as a function of the number of BP layers. With the increase in the number of BP layers (1 to 9), the maximum sensitivity is found to be 275.2 Degree/RIU) with eight BP layers (B = 8). After eight layers, the sensitivity decreases. This decrement in value is because the utilization rate of light wave decrements with enhancing the number of BP layers.

The next plot (Fig. 5b) gives the impact of the number of PtSe$_2$ layers on the sensor sensitivity. The plot is not following the same trend as in Fig. 5a; it is decrementing after the second layer. The peak value of sensitivity is found to be 215 Degree/RIU) at P = 2. So, with these discussions, we conclude that the optimization of the BP

layer is done, followed by the optimization of the PtSe$_2$ layer. Tand the maximum sensitivity we are getting is 275.2 Degree/RIU) (for P = 1, B = 8). Using constant angular interrogation, various plots have been drawn for conclusive evidence. Multiple Y-axis parameters (FWHM and minimum reflectivity) with a single X-axis showing sensitivity are plotted for variable BP layers [0 to 8] with mono (P = 1)-layer of PtSe$_2$ (Fig. 6a) at RI of sensing layer 1.38. The minimum and maximum sensitivity values attained were 180.2 Degree/RIU) and 275.2 Degree/RIU), with values of minimum reflectance and FWHM varying from 0.07129 to 0.23796 and 4.73 Degree to 6.38 Degree, respectively. Figure 6b shows the sensitivity's functional relationship between DA and FoM. The number of layers taken is the same as in the previous case. The highest values obtained with this plot for both parameters [DA

and FoM] were 0.21 to 0.16 and 38.1 to 43.1, respectively. It depicts that the electric field distribution at the highest sensitivity is accurate and sharper, while vice versa in the lowest sensitivity value. Next, in Fig. 6c, the plots for DA and FoM are plotted concerning the sensor sensitivity. These parameter calculations were done taking constant BP layer ($B = 1$) and varying $PtSe_2$ layers (0 to 2).

The maximum sensitivity, FoM, and DA were calculated as 215 Degree/RIU, 36.1 RIU^{-1}, and 0.17 $Degree^{-1}$. Similarly, with Fig.6d, the maximum values of FWHM and minimum reflectance (R_{min}) come out to be 5.95 Degree and 0.32291.

Figure 7 depicts the relation of electric field distribution inside the sensor with the distance of the prism interface. At the Ag-$PtSe_2$ boundary, the electric field intensity increases, which further increases at the $PtSe_2$-BP boundary. After the last boundary of the BP-sensing medium, its value decreases exponentially. It was observed that when light absorption is greater, field intensity enhances. It demonstrates that higher light absorption causes considerable SPW excitation. Figure 7a–c shows the electric field distribution plots for the three cases of thickness, D_2 of $PtSe_2$ as 2 nm, 3.3 nm, and 4.4 nm. In the upcoming Table 2, a comparison is made with similar previous reported works, and an analysis is made with the help of performance parameters like sensitivity, DA, and FoM. This paper's results show that the achieved sensitivity and FoM are higher than in earlier works.

4 Conclusion

Finally, we theoretically studied a novel form of sensor structure based on the Kretschmann configuration with the addition of a $PtSe_2$ and a BP layer. The inclusion of $PtSe_2$ and the BP layer has been discovered to be beneficial as it increases the overall performance of the SPR sensor. We have analyzed the results showing that the sensor's sensitivity may increase using the proposed design. By altering the number of BP layers in the design, the sensitivity can be improved to a maximum of 275.2 Degree/RIU. Our study gives a positive sign of more research exploration in bio-sensing-based applications giving high-performance parameters.

Declarations

Conflict of interest The authors declare that they have no confict of interest.

Ethical approval Not applicable. The work presented in this manuscript is mathematical modeling only for the proposed biosensor. No experiment was performed on the human body and/or living organism/animal. So, ethical approval from an ethical committee is not required.

Consent to participate The author willing to participate in the work presented in this manuscript.

Consent for publication The author has given their consent to publish this work.

References

1. Zhang, Y., et al.: Plasmonic tweezers: for nanoscale optical trapping and beyond. Light Sci. Appl. (2021). https://doi.org/10.1038/s41377-021-00474-0
2. Zhang, J., Zhang, L., Xu, W.: Surface plasmon polaritons: physics and applications. J. Phys. D. Appl. Phys. (2012). https://doi.org/10.1088/0022-3727/45/11/113001
3. Kashyap, R., et al.: Enhanced biosensing activity of bimetallic surface plasmon resonance sensor. Photonics (2019). https://doi.org/10.3390/photonics6040108
4. Purohit, B., Vernekar, P.R., Shetti, N.P., Chandra, P.: Biosensor nanoengineering: Design, operation, and implementation for biomolecular analysis. Sensors Int. (2020). https://doi.org/10.1016/j.sintl.2020.100040
5. Chen, J., et al.: Optical cavity-enhanced localized surface plasmon resonance for high-quality sensing. IEEE Photon. Technol. Lett. **30**(8), 728–731 (2018). https://doi.org/10.1109/LPT.2018.2814216
6. De Melo, A.A., Da Silva, T.B., Da Silva Santiago, M.F., Da Silva Moreira, C., Cruz, R.M.S.: Theoretical analysis of sensitivity enhancement by graphene usage in optical fiber surface plasmon resonance sensors. IEEE Trans. Instrum. Meas. **68**(5), 1554–1560 (2019). https://doi.org/10.1109/TIM.2018.2882148
7. Hajshahvaladi, L., Kaatuzian, H., Danaie, M.: A high-sensitivity refractive index biosensor based on Si nanorings coupled to plasmonic nanohole arrays for glucose detection in water solution. Opt. Commun. (2022). https://doi.org/10.1016/j.optcom.2021.127421
8. Karabchevsky, A., Tsapovsky, L., Marks, R.S., Abdulhalim, I.: Study of immobilization procedure on silver nanolayers and detection of estrone with diverged beam surface plasmon resonance (SPR) imaging. Biosensors **3**(1), 157–170 (2013). https://doi.org/10.3390/bios3010157
9. Meshginqalam, B., Barvestani, J.: Performance enhancement of SPR biosensor based on phosphorene and transition metal dichalcogenides for sensing DNA hybridization. IEEE Sens. J. **18**(18), 7537–7543 (2018). https://doi.org/10.1109/JSEN.2018.2861829
10. Wang, Q., Sun, B., Hu, E., Wei, W.: Cu/ITO-coated uncladded fiber-optic biosensor based on surface plasmon resonance. IEEE Photonics Technol. Lett. **31**(14), 1159–1162 (2019). https://doi.org/10.1109/LPT.2019.2908288
11. Pal, A., Jha, A.: A theoretical analysis on sensitivity improvement of an SPR refractive index sensor with graphene and barium titanate nanosheets. Optik (Stuttg) (2021). https://doi.org/10.1016/j.ijleo.2021.166378
12. Uniyal, A., Chauhan, B., Pal, A., Singh, Y.: Surface plasmon biosensor based on Bi 2 Te 3 antimonene heterostructure for the detection of cancer cells. Appl. Opt. **61**(13), 3711–3719 (2022)
13. Jia, Y., Li, Z., Wang, H., Saeed, M., Cai, H.: Sensitivity enhancement of a surface plasmon resonance sensor with platinum

diselenide. Sensors (Switzerland) (2020). https://doi.org/10.3390/s20010131

14. Xiang, Y., Zhu, J., Wu, L., You, Q., Ruan, B., Dai, X.: Highly sensitive terahertz gas sensor based on surface plasmon resonance with graphene. IEEE Photon. J. **10**(1), 1–7 (2018). https://doi.org/10.1109/JPHOT.2017.2778245

15. Rahman, M.S., Anower, M.S., Abdulrazak, L.F.: Modeling of a fiber optic SPR biosensor employing Tin Selenide (SnSe) allotropes. Results Phys. (2019). https://doi.org/10.1016/j.rinp.2019.102623

16. Nangare, S., Patil, P.: Black phosphorus nanostructure based highly sensitive and selective surface plasmon resonance sensor for biological and chemical sensing: a review. Crit. Rev. Anal. Chem. (2021). https://doi.org/10.1080/10408347.2021.1927669

17. Yu, H., Peng, Y., Yang, Y., Li, Z.Y.: Plasmon-enhanced light–matter interactions and applications. npj Comput Mater. **5**(1), 1–14 (2019). https://doi.org/10.1038/s41524-019-0184-1

18. Xia, L., Yin, S., Gao, H., Deng, Q., Du, C.: Sensitivity enhancement for surface plasmon resonance imaging biosensor by utilizing gold-silver bimetallic film configuration. Plasmonics **6**(2), 245–250 (2011). https://doi.org/10.1007/s11468-010-9195-y

19. Otto, A.: Excitation of nonradiative surface plasma waves in silver by the method of frustrated total reflection. Zeitschrift für Phys. **216**(4), 398–410 (1968). https://doi.org/10.1007/BF01391532

20. Vasudevan Pillai Radha, S., Santhakumari Amma Ravindran Nair, S.K., Sankaranarayana Iyer, S.: Surface plasmon resonance-based fiber-optic metallic multilayer biosensors. ACS Omega **6**(23), 15068–15077 (2021). https://doi.org/10.1021/acsomega.1c01236

21. Karki, B., Uniyal, A., Chauhan, B., Pal, A.: Sensitivity enhancement of a graphene, zinc sulfide-based surface plasmon resonance biosensor with an Ag metal configuration in the visible region. J. Comput. Electron. (2022). https://doi.org/10.1007/s10825-022-01854-4

22. Zhang, P., Wang, J., Chen, G., Shen, J., Li, C., Tang, T.: A high-sensitivity spr sensor with bimetal/silicon/two-dimensional material structure: a theoretical analysis. Photonics (2021). https://doi.org/10.3390/photonics8070270

23. Saifur Rahman, M., Anower, M.S., Bin Bashar, L., Rikta, K.A.: Sensitivity analysis of graphene coated surface plasmon resonance biosensors for biosensing applications. Sens. Bio-Sensing Res. **16**, 41–45 (2017). https://doi.org/10.1016/j.sbsr.2017.11.001

24. Singh, Y., Kumar, M., Sanjeev, P., Raghuwanshi, K.: Sensitivity Enhancement of SPR Sensor with the Black Phosphorus and Graphene with Bi-layer of Gold for Chemical Sensing. Plasmonics (2021). https://doi.org/10.1007/s11468-020-01315-3

25. Koppens, F.H.L., Chang, D.E., García De Abajo, F.J.: Graphene plasmonics: a platform for strong light-matter interactions. Nano Lett. **11**(8), 3370–3377 (2011). https://doi.org/10.1021/nl201771h

26. Castellanos-Gomez, A.: Black phosphorus: narrow gap, wide applications. J. Phys. Chem. Lett. **6**(21), 4280–4291 (2015). https://doi.org/10.1021/acs.jpclett.5b01686

27. Pumera, M.: Phosphorene and black phosphorus for sensing and biosensing. TrAC Trends Anal. Chem. **93**, 1–6 (2017). https://doi.org/10.1016/j.trac.2017.05.002

28. Cen, C., et al.: High quality factor, high sensitivity metamaterial graphene—perfect absorber based on critical coupling theory and impedance matching. Nanomaterials (2020). https://doi.org/10.3390/nano10010095

29. Singh, S., et al.: 2D nanomaterial-based surface plasmon resonance sensors for biosensing applications. Micromachines **11**(8), 1–28 (2020). https://doi.org/10.3390/mi11080779

30. Y. Cai, G. Zhang, and Y. Zhang, "Layer-dependent Band Alignment and Work Function of Few-Layer Phosphorene," pp. 1–19.

31. Rahman, M.M., Rana, M.M., Rahman, M.S., Anower, M.S., Mollah, M.A., Paul, A.K.: Sensitivity enhancement of SPR biosensors employing heterostructure of PtSe2 and 2D materials. Opt. Mater.

(Amst) **107**, 110123 (2020). https://doi.org/10.1016/j.optmat.2020.110123

32. Fouad, S., Sabri, N., Jamal, Z.A.Z., Poopalan, P.: Enhanced sensitivity of surface plasmon resonance sensor based on bilayers of silver-barium titanate. J. Nano-Electron. Phys. **8**(4), 2–6 (2016). https://doi.org/10.21272/jnep.8(4(2)).04085

33. Srivastava, T., Jha, R.: Black phosphorus: a new platform for gaseous sensing based on surface plasmon resonance. IEEE Photon. Technol. Lett. **30**(4), 319–322 (2018). https://doi.org/10.1109/LPT.2017.2787057

34. Kumela, A.G., Gemta, A.B., Desta, T.A., Kebede, A.: Noble classical and quantum approach to model the optical properties of metallic nanoparticles to enhance the sensitivity of optoplasmonic sensors. RSC Adv. **12**(25), 16203–16214 (2022). https://doi.org/10.1039/d2ra00824f

35. Wang, Y.Q.Y., et al.: Monolayer PtSe2, a new semiconducting transition-metal- dichalcogenide, epitaxially grown by direct selenization of Pt. Nano Lett. **8**(15), 4013–4018 (2015). https://doi.org/10.21272/jnep.8(4(2)).04085

36. Uniyal, A., Chauhan, B., Pal, A., Srivastava, V.: InP and graphene employed surface plasmon resonance sensor for measurement of sucrose concentration : a numerical approach. Opt. Eng. **61**(May), 1–13 (2022). https://doi.org/10.1117/1.OE.61.5.057103

37. Karki, B., Sharma, S., Singh, Y., Pal, A.: Sensitivity enhancement of surface plasmon resonance biosensor with 2-D franckeite nanosheets. Plasmonics **13**, 1–16 (2021)

38. Daher, M.G., Taya, S.A., Colak, I., Patel, S.K., Olaimat, M.M.: Surface plasmon resonance biosensor based on graphene layer for the detection of waterborne bacteria. J. Biophotonics **15**(5), 1–9 (2022). https://doi.org/10.1002/jbio.202200001

39. Karki, B., Pal, A., Singh, Y., Sharma, S.: Sensitivity enhancement of surface plasmon resonance sensor using 2D material barium titanate and black phosphorus over the bimetallic layer of Au, Ag, and Cu. Opt. Commun. (2021). https://doi.org/10.1016/j.optcom.2021.127616

40. Karki, B., Trabelsi, Y., Uniyal, A., Pal, A.: Zinc sulfide, silicon dioxide, and black phosphorus based ultra-sensitive surface plasmon biosensor. Opt. Quantum Electron. (2022). https://doi.org/10.1007/s11082-021-03480-z

41. Karki, B., Uniyal, A., Pal, A., Srivastava, V.: Advances in surface plasmon resonance-based biosensor technologies for cancer cell detection. Int. J. Opt. (2022). https://doi.org/10.1016/j.bios.2021.113767

42. Bhishma Karki, B., Vasudevan, A.U., Pal, A., Srivastava, V.: Hemoglobin detection in blood samples using a graphene-based surface plasmon resonance biosensor. Optik **270**, 169947 (2022). https://doi.org/10.1016/j.ijleo.2022.169947

43. Karki, B., Ramya, K.C., Devi, R.S.S., Srivastava, V., Pal, A.: Titanium dioxide, black phosphorus and bimetallic layer-based surface plasmon biosensor for formalin detection: numerical analysis. Opt. Quantum Electron. (2022). https://doi.org/10.1007/s11082-022-03875-6

44. Kumar, R., Kushwaha, A.S., Srivastava, M., Mishra, H., Srivastava, S.K.: Enhancement in sensitivity of graphene-based zinc oxide assisted bimetallic surface plasmon resonance (Spr) biosensor. Appl. Phys. A Mater. Sci. Process. **124**(3), 1–10 (2018). https://doi.org/10.1007/s00339-018-1606-5

45. Nurrohman, D.T., Chiu, N.-F.: Surface plasmon resonance biosensor performance analysis on 2D material based on graphene and transition metal dichalcogenides. ECS J. Solid State Sci. Technol. **9**(11), 115023 (2020). https://doi.org/10.1149/2162-8777/abb419

46. Srivastava, A., Prajapati, Y.K.: Performance analysis of silicon and blue phosphorene/mos2 hetero-structure based SPR sensor. Photonic Sensors **9**(3), 284–292 (2019). https://doi.org/10.1007/s13320-019-0533-1

47. Nur, J.N., Hasib, M.H.H., Asrafy, F., Shushama, K.N., Inum, R., Rana, M.M.: Improvement of the performance parameters of the surface plasmon resonance biosensor using Al2O3 and WS2. Opt. Quantum Electron. **51**(6), 1–11 (2019). https://doi.org/10.1007/s11082-019-1886-9

48. Lin, Z., et al.: Tuning and sensitivity enhancement of surface plasmon resonance biosensor with graphene covered Au-MoS2-Au films. IEEE Photon. J. (2016). https://doi.org/10.1109/JPHOT.2016.2631407